Journal of Materials Chemistry C

Accepted Manuscript

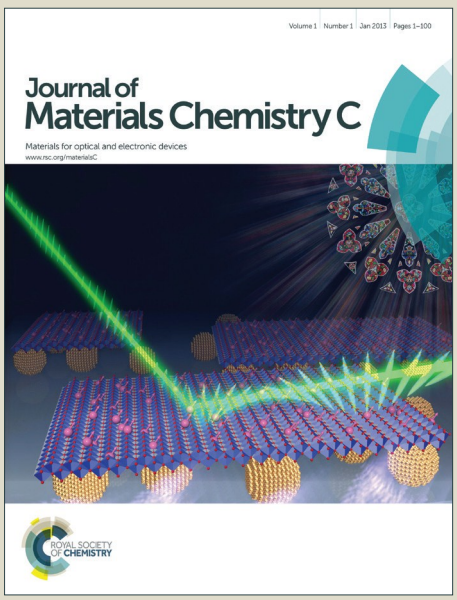

ROYAL SOCIETY OF CHEMISTRY

www.rsc.org/materialsC

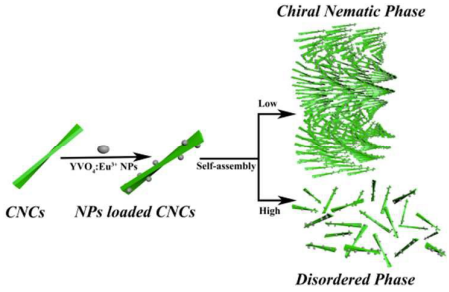

Hierarchical chiroptical activity of the emissive $YVO_4:Eu^{3+}$ nanoparticles in chiral nematic cellulose host matrix.

Cite this: DOI: 10.1039/c0xx00000x

www.rsc.org/xxxxxx

ARTICLE TYPE

Chiral Electronic Transitions of $YVO_4:Eu^{3+}$ Nanoparticles in Cellulose based Photonic Materials with Circularly Polarized Excitation

Guang Chu[a], Xuesi Wang[b], Tianrui Chen[a], Wen Xu[b], Yu Wang[*a], Hongwei Song[b] and Yan Xu[*a]

Received (in XXX, XXX) Xth XXXXXXXXX 20XX, Accepted Xth XXXXXXXXX 20XX

DOI: 10.1039/b000000x

A novel chiral nematic luminescence film is fabricated by incorporating the $YVO_4:Eu^{3+}$ nanoparticles with cellulose nanocrystals. We have shown that these nanoparticles could attach to the surface of twisted nanorods of cellulose, exhibiting electronic transition-based hierarchical chiroptical activity, responsible for strong circularly polarized emission and high luminescence polarization dissymmetry factor.

Introduction

Circularly polarized excitation (CPE) reflects the chirality of materials in ground-state structural features, as a particularly sensitive technique has attracted considerable attention due to its high specificity and potential applications in the photonic devices, such as light-emitting diodes, optical amplifiers and information storage.[1-6] The omnipresence of chirality demands urgent development of circularly polarized luminescence microscopes making exploration of chiral environments an easy task.[7] Chiral liquid crystals are smart stimulus-responsive materials with promising applications in chiral photonics.[8] A hybrid system of chiral liquid crystal materials doped with fluorescent species has been discovered, and the emission is found to be circularly polarized to an extend that depends on the degree of alignment of the guest luminophor within host matrix.[9-11] As we know, the rare-earth doped nanoparticles (NPs) have good hydrothermal stability as well as rich emission spectrum due to their unique *4f-4f* inner-shell electron transitions,[12] chiral assembly of them could give rise to a chiral electronic transition combining with interesting CPE properties.

Cellulose nanocrystals (CNCs), which can be obtained by acid-hydrolysis of bulk cellulose,[13] have garnered a tremendous attention in the materials science because of their unsurpassed quintessential physical and chemical properties[14, 15]. CNCs have high mechanical strength, optical transparency and excellent dispersibility in water. During low concentration, they can form a chiral nematic lyotropic liquid crystal phase with locally uniform orientation of the rods along a common direction, which can be preserved upon air-drying, resulting in iridescent films. A chiral nematic film of CNCs with helical pitch as short as the wavelength of visible lights exhibits strong circular dichrosim (CD).[16] The band-gap position for the chiral nematic CNCs can be tuned from visible to near-infrared light region by changing preparation conditions, such as ultrasonic treatment and adding salt[17-19]. The chiral nematic ordering of CNCs can be transferred to inorganic materials through replicating and imprinting as demonstrated by prior work.[20, 21] Organization of rare-earth doped luminescence NPs into the chiral nematic matrix of CNCs has, to the best of our knowledge, not yet been reported.

Here we present a straightforward and cost-effective approach to fabricating the chiroptical luminescence hybrid films by incorporating $YVO_4:Eu^{3+}$ NPs into the chiral nematic matrix of CNCs, designated as CY films. The CY films exhibit unique CPE properties due to the combined merits of rare-earth doped NPs and chiral photonic structure of CNCs. The $YVO_4:Eu^{3+}$ NPs could adsorb on the surface of CNCs nanorods, giving rise to a strong electronic transitions-based CD signal, stronger in CY films than that in the mixed solution. The CD signals of the CY films can be modulated by varying the $YVO_4:Eu^{3+}$ NPs loading and with the aid of ultrasound treatment.

Experimental Section

Materials and characterization

All Chemicals were used as received without further purification. Europium nitrate hexahydrate ($Eu(NO_3)_3{\cdot}6H_2O$, 99.9%), yttrium nitrate hexahydrate ($Y(NO_3)_3{\cdot}6H_2O$, AR) and sodium orthovanadate ($NaVO_4{\cdot}12H_2O$, 99.9%) were purchased from Aladin Industry corporation. Sodium citrate ($C_6H_5Na_3O_7$, 99%) and sodium hydroxide (NaOH, AR) were purchased from Beijing Chemical Works. Cotton pulp board was purchased from Hebei Paper Group of China.

Powder X-ray diffraction (XRD) patterns were recorded using a Rigaku D/Max 2550 X-ray diffractometer (Cu K radiation, λ = 1.5406 Å). Surface morphologies were characterized using JEOL-6700 F field emission scanning electron microscope (SEM) at an accelerating voltage of 3 KV. Transmission electron microscopy (TEM) and high resolution transmission electron microscopy (HRTEM) were conducted on a FEI Tecnai G2S-Twin with a field emission gun operating at 200 KV. Transmission UV-visible spectroscopy was carried out on a Shimazu UV-1800 UV-Visible spectrophotometer. Spectra were collected by mounting free-standing films so that the surfaces of the films were perpendicular to the beam path. Circular dichroism (CD) spectra were recorded on a BioLogic MOS-450 spectropolarimeter and the solid samples were mounted normal to

Cite this: DOI: 10.1039/c0xx00000x

www.rsc.org/xxxxxx

ARTICLE TYPE

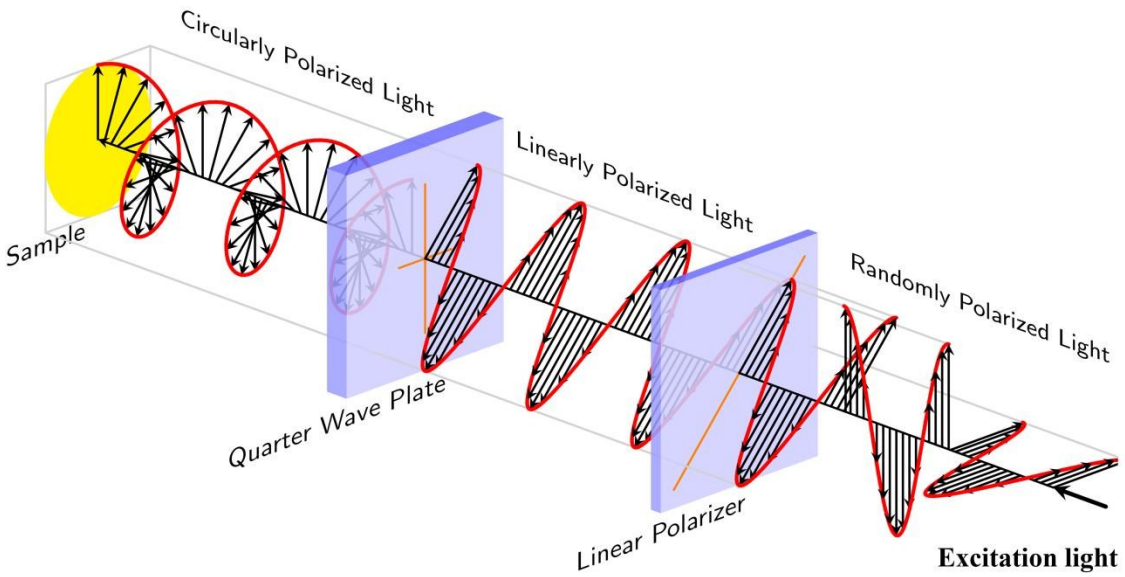

Scheme 1 Schematic illustration of the home-made left/right- handed circularly polarized optical set up for the CPE spectra.

the beam. Polarized optical microscopy (POM) image was conducted on Olympus BX51-P microscope with images taken by polarizers in a perpendicular arrangement. Zeta potential was measured on Malvern Zetasizer Nano-ZS90. The fourier transform infrared spectrum (FTIR) was conducted on Bruker IFS 66v/S spectrometer. Photoluminescence spectra were recorded on FluoroMax-4 fluorescence spectrophotometer (Horiba Scientific) equipped with a 450 W Xe-arc lamp and a home-built laser system consisting of a Nd:YAG pumping laser operating at 465 nm for fluorescence excitation, the third-order harmonic generator (355 nm), and a tunable optical parameter oscillator (OPO, Continuum Precision II 8000). It has pulse duration of 10 ns, repetition frequency of 10 Hz, and line width of 4-7cm^{-1}. The direction of detection was normal to the film surface, whereas the excitation beam from the opposite side of the film was oriented at a certain angle to the normal. The circularly polarized excitation (CPE) spectra were obtained using a combination of a linear polarizer with a broad-band quarter-wave plate (Scheme 1).

Preparation of hybrid chiral nematic films of CNCs and YVO_4:Eu^{3+} NPs

The preparation of CNCs and YVO_4:Eu^{3+} NPs was accomplished according to the reported procedures[22, 23], with the experiment details given in the Supporting Information. Two above-mentioned aqueous suspensions, one comprising YVO_4:Eu^{3+} NPs (0.03 M) and the other one alkaline CNCs (3.5 wt%), were mixed with varying volume ratios of CNCs-to-NPs (Table S1). The mixed solution was stirred at ambient temperature for 30 min to give rise to a homogeneous mixture. Then, the mixture was poured into polystyrene Petri dishes (60 mm), followed by evaporation under ambient conditions for 2 days giving rise to a free-standing iridescent hybrid chiral nematic film of CNCs and YVO_4:Eu^{3+} NPs. For the purpose of comparison, the NPs-free chiral nematic film of CNCs was prepared under the same conditions by using alkaline CNCs suspension only.

Results and discussions

General structural features of the CY films

The hybrid chiral nematic films of CNCs and YVO_4:Eu^{3+} NPs are prepared by evaporation-induced co-assembly approach at room temperature from 3.5 wt% aqueous alkaline suspension of CNCs and 0.03 M aqueous solution of YVO_4:Eu^{3+} at varying volume ratios (Table S1). CNCs have rod morphology with an average length and diameter of 200-300 nm and 15-20 nm, respectively (Fig. 1a). YVO_4:Eu^{3+} NPs have an average size of around 7 nm (Fig. 1b), in agreement with the estimated size based on Scherrer's method (Fig. S1). The YVO_4:Eu^{3+} NPs are crystalline, and all diffraction peaks on the XRD pattern can be indexed to a tetragonal phase (JCPDS 17-0341). The average *d*- spacing of the lattice fringes measured from the HRTEM image is about 0.14 nm, agreeing with the d_{202} lattice plane of tetragonal, YVO_4 (Fig. S2). Firstly, we tested whether the CNCs-YVO_4:Eu^{3+} NPs mixtures could form a chiral nematic phase by drop-casting the mixtures into a liquid crystal cell and observing the evaporation process through POM technique. As evaporation takes place, mass of fingerprint textures are established, demonstrating the formation of chiral nematic phase of CNCs over the YVO_4:Eu^{3+} NPs loadings (Fig. 1c). The periodic spacing between two adjacent fingerprint texture is defined as half helical pitch.[24] On the high magnification SEM images of the CY films, a large area of periodic arrangement is observed, indicating the helical

Cite this: DOI: 10.1039/c0xx00000x

www.rsc.org/xxxxxx

ARTICLE TYPE

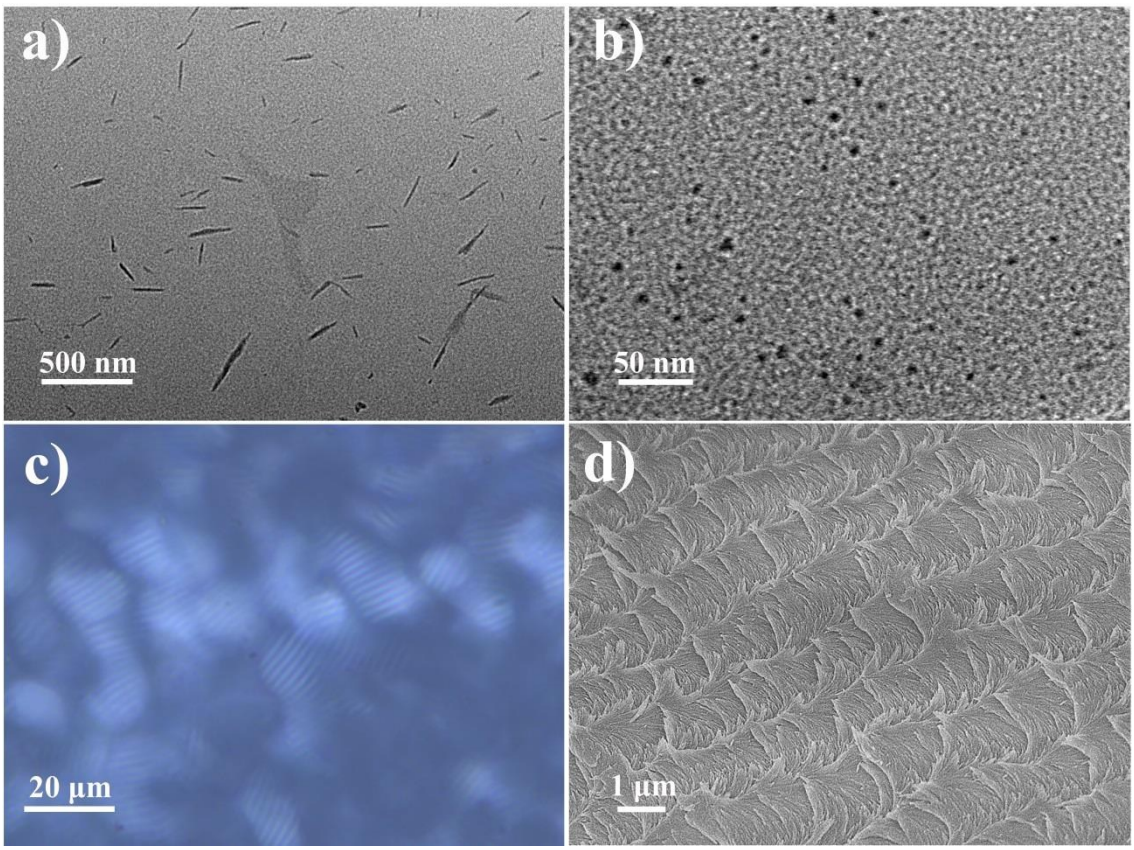

Fig. 1 (**a**) TEM image of CNCs nanorods, (**b**) TEM image of YVO_4:Eu^{3+} NPs. (**c**) POM micrograph of a drop taken from a CNCs/YVO_4:Eu^{3+} NPs mixture during evaporation into a liquid crystal cell. (**d**) Magnified SEM image of CY1b showing a large area of periodic chiral arrangement of the host CNCs rods.

order of CNCs suspension can be preserved in a condense phase upon complete drying of a thin film (Fig. 1d). The solid CNCs host matrix is tunable for its helical pitch with corresponding value of 1.5 (CY1b), 1.8 (CY2b) and 2.2 µm for CY3b respectively (measured by POM technique), which prove that ultrasonic treatment can effectively change the helical pitch of the chiral nematic cellulose films.[18, 19]

A change in birefringence from blue to yellow for CY1b, CY2b and CY3b based on the photograph images confirming an increase in helical pitch (Fig. 2a). The NPs loading of these composites remain the same, the change of iridescence come from the host chiral nematic arrangement of the CNCs. It is interesting to note that these chiral nematic films appear to have the same red luminescence with similar brightness when viewed under UV light (Fig. 2b). POM images of the CY films show birefringent textures with a red-colored shift relative to the corresponding composites, indicating the anisotropy of the material (Fig. 2c-2e). The transmittance spectra of the corresponding CY films exhibit characteristic photonic property with the band-gap centered at 342 nm, 472 nm and 550 nm, respectively (Fig. 2f). The distortion in the transmittance spectrum of CY1b is likely due to the overlap and coupling between the band-gap and the absorption of YVO_4:Eu^{3+} NPs (Fig. S3).

Increasing NPs loading results in a decrease in helical pitch, and corresponding blue-shift and ultimate disappearance of the band-gap based on the transmittance spectral analysis (Fig. S4). Over-loading of the YVO_4:Eu^{3+} NPs causes loss of chiral nematic organization based on the POM and SEM imaging analysis (Fig. S5). This observation is similar to prior observations that addition of electrolyte to CNCs suspension, where the increased ionic strength can change the electrostatic double layers of the CNCs, which induce the increase of the helical twisting power of the CNCs.[18, 19]

Hierarchical chiroptical activity of the CY films

CD is a common phenomenon found in optically active chiral materials due to the adsorption difference between right- and left-circularly polarized light. It is well known that the oriented solid films could exhibit both linear dichroism and birefringence properties. The linear dichroism/birefringence possibility of the CY samples can be eliminated by measuring samples at various

azimuthal orientations perpendicular to the light beam and the "front-and-back" CD measurements (Fig. S6). Fig.3a shows the CD spectra of the CY films prepared under static and ultrasonic conditions, respectively. For these samples, they exhibit two spectral bands with the same chirality. The larger peaks are centered at 380 nm, 510 nm and 560 nm, respectively, derived from the chiral photonic structure, which coincides to their UV spectra (Fig.3d, Fig.2f). The smaller peaks in CD spectra are in the position of 340 nm, approaching to the adsorption of YVO_4:Eu^{3+} NPs (Fig. S3), and their corresponding UV spectra show strong adsorption at the range of 340 nm, responsible for the guest YVO_4:Eu^{3+}NPs in CNCs host matrix (Fig.3d). As we know, chirality may be imparted from the CNCs template at three different length scales: (i) molecular chirality of the D-glucose units; (ii) morphologic chirality of the screw-shaped CNCs; (iii) chiral nematic long-range order of the supramolecular assembly of CNCs.[25] As the chiral biomolecules only absorb in the far ultraviolet region (less than 250 nm), the CD activity at 340 nm can only be assigned to excitation of states in the inorganic material, thus chiral electronic transition of YVO_4:Eu^{3+} NPs.

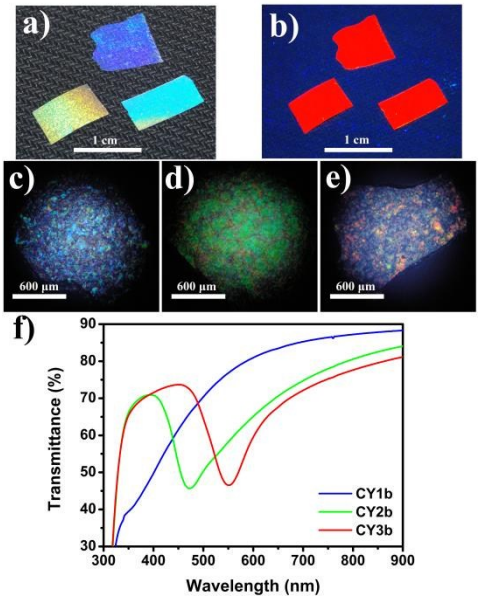

Fig. 2 (**a**) Photograph of CY1b, CY2b and CY3b showing tunable blue-to-yellow iridescence. (**b**) Photograph of the CY films viewed under UV light shows red emission. POM images of the chiral nematic CY films: (**c**) CY1b, (**d**) CY2b and (**e**) CY3b, respectively. (**f**) UV-vis spectra of the CY films.

The effect of NPs loading on the chiroptical activity of the CY films has been investigated, along with the NPs-free cellulose as a reference (Fig. 3b). The latter shows a positive unimodal CD peak, typical for its chiral nematic nature. At low NPs content (CY3b-c), the spectra of CY film shows a strong positive CD signal, which can be ascribed to the chiral matrix of CNCs combined with the chiral electronic transition of YVO_4:Eu^{3+} NPs. When with excess NPs exist in the composite films (CY3d-f), the CD signal changes into a positive broad band belonging to the chiral excitation of NPs, while the signal belonging to the photonic structure of CNCs matrix disappeared which indicates the completely disappearance of the chiral nematic structure. In previous studies, the relative chiral arrangement of the inorganic NPs can result in a chiral excitation CD signal.[26-28] This inspired us that these NPs maybe attach to the chiral rods of CNCs, give rise to a screw-like arrangement. Additionally, the corresponding UV spectra of these samples fit well with their CD signal during the same wavelength range (Fig. 3e), indicating that the chiroptical activity of the NPs originates in the chiral arrangement of the NPs itself, not the artefact on CD spectra.

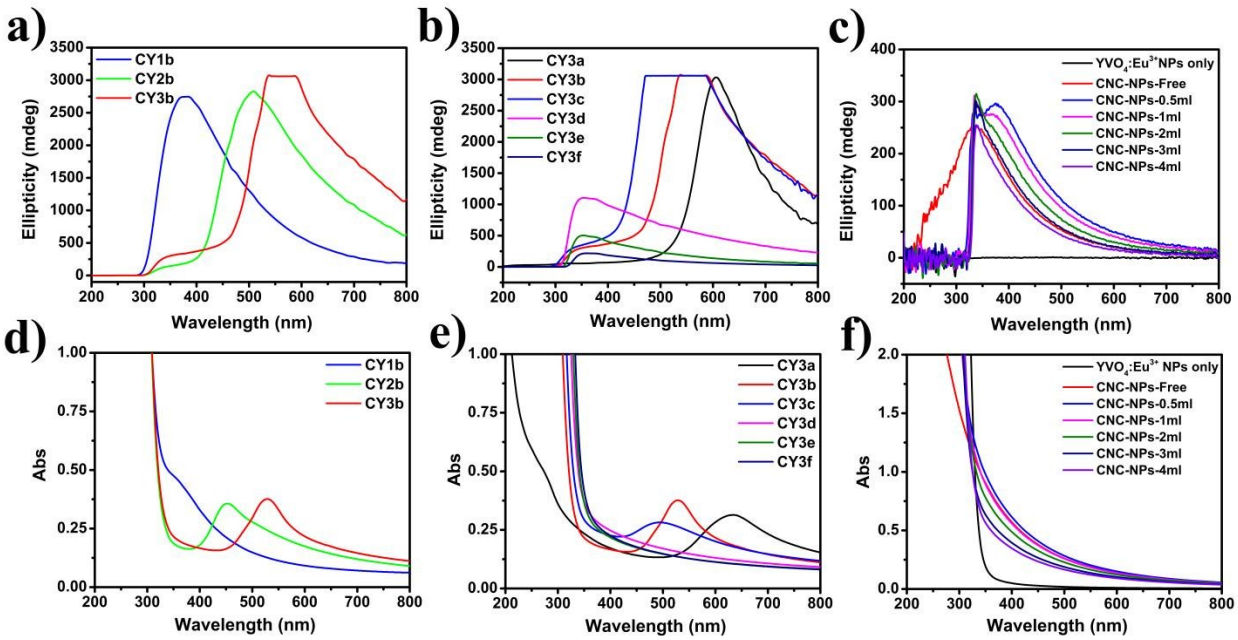

Fig. 3 (**a**) The CD spectra of chiral nematic CY films prepared under static condition for CY1b and ultrasonic conditions of different power for CY2b and CY3b, showing different helical pitches. (**b**) The CD spectra of the CY film with varying amount of NPs. (**c**) The CD spectra of the mixed solution of CNCs and NPs. The corresponding UV-Vis spectra of these samples are shown in (**d**), (**e**) and (**f**), respectively. The thickness of the CY films is about 0.5 mm. Some of the spectra appear cut off since the peak is greater than the maximum detectable signal on the spectropolarimeter that was used.

The CD spectrum of the mixed solution containing varying amount of YVO_4:Eu^{3+} NPs has also been studied, along with the individual CD spectrum of YVO_4:Eu^{3+} NPs solution and CNCs suspension (Fig. 3c). The YVO_4:Eu^{3+} NPs solution shows no CD response, confirming the NPs are achiral. And the intense single CD peak for the CNCs suspension arises primarily from the scattering of chiral shape of CNCs. Interestingly, the CD signal belongs to the D-glucose units (bellow 300 nm) disappeared with the addition of NPs, which may due to the attachment of the NPs to the surface of CNCs rods, of which is confirmed by the TEM image of the mixed suspension of YVO_4:Eu^{3+} NPs doped with CNCs on dry state (Fig. S7). Mixtures of the YVO_4:Eu^{3+} NPs solution and CNCs suspension containing varying amount of the NPs solution exhibit concentration-dependent CD responses in a way that differ from that of the CY films. At low NPs content, the mixed solution exhibit two signals: one associate with the chiral shape scattering of the CNCs and the other one with the chiral excitation of YVO_4:Eu^{3+} NPs (a sharp peak at 340 nm). With the increasing of NPs concentration, the shape of the CD spectra changes into a sharp spike which corresponding to YVO_4:Eu^{3+} NPs. No CD signal corresponding to the chiral shape of CNCs is observed. The CD spectra confirm that the hydrogen bond and van der Waals interaction may occur between the CNCs rod and YVO_4:Eu^{3+} NPs. In addition, the UV spectra of the corresponding mixtures are presented in Fig. 3f. The coupled absorption signal is at the range of 340 nm, which confirms the chiral electronic transition of NPs combined with CNCs nanorods.

In order to further prove the interaction between CNCs and YVO_4:Eu^{3+} NPs, Fig. 4 shows the FTIR spectra of the CNCs, NPs loaded CNCs and YVO_4:Eu^{3+} NPs only, respectively. For YVO_4:Eu^{3+} NPs, the transmittance band around 823 cm^{-1} is ascribed to the V-O stretching vibration in the VO_4 tetrahedron. The band at 1571 and 3392 cm^{-1} can be assigned to the OH^- bending and stretching modes. For CNCs rods, the peak at 2898 cm^{-1} is corresponding to C-H stretching vibration in D-glucose

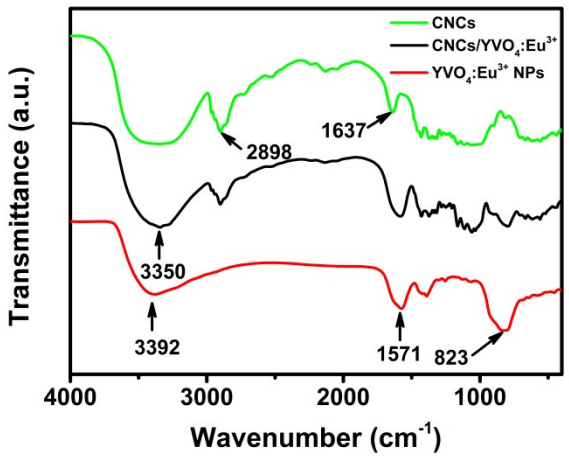

Fig. 4 FTIR spectra of the CNC nanorods, NPs loaded CNC and YVO_4:Eu^{3+} NPs only, respectively.

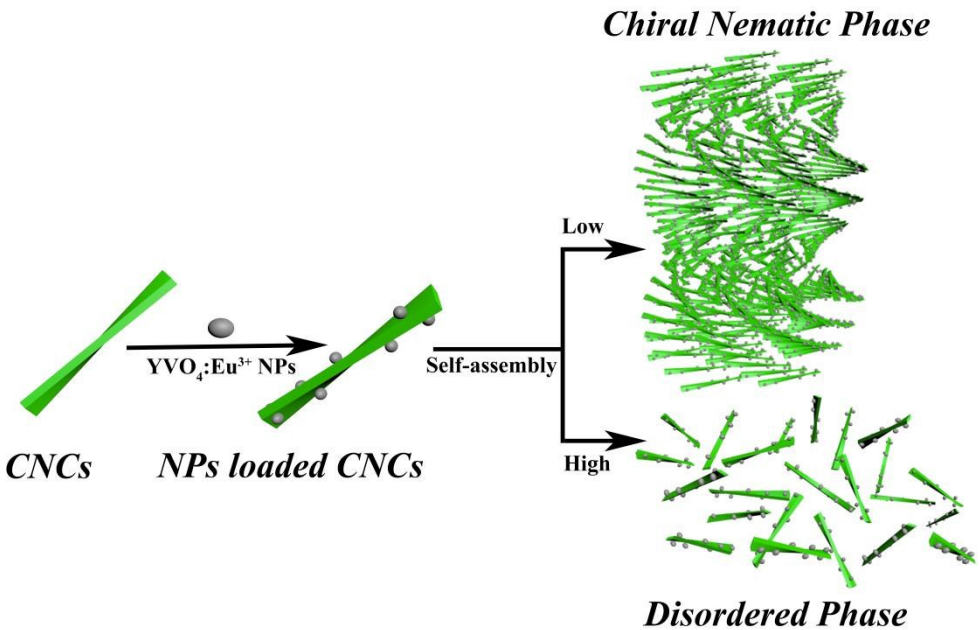

Scheme 2 Schematic illustration of the co-assembly approach of CNC chiral rod and YVO_4:Eu^{3+} NPs.

units, and the peak at 1637 cm^{-1} can be ascribed to the C=O stretching. And the obviously broad band at 3550-3220 cm^{-1} can be assigned to the OH^- groups, is characteristic of intermolecular hydrogen bond between D-glucose units. However, in the sample of NPs loaded CNCs, a combined vibration bands of both CNCs and YVO_4:Eu^{3+} NPs appears, furthermore, the shape of the OH^- bending and stretching band at 3350 cm^{-1} becomes narrow, as well as a little shift comparing with the pure CNCs and NPs, which means a interaction occurs between CNCs and YVO_4:Eu^{3+} NPs, suggesting the attachment of NPs to the surface of CNCs rod due to the hydrogen bond.

On the basis of the above-mentioned results, an artist view of the possible approach to the preparation of chiral nematic luminescence films is depicted in Scheme 2. The anionic charged CNCs nanorods were obtained by hydrolysis in sulfuric acid that reacting with the surface hydroxyl groups of cellulose to yield surface sulfate esters with zeta potential of -22.3 mV. YVO_4:Eu^{3+} NPs carry negative charges with zeta potential of -27.4 mV which

could match to the CNCs and stable in weak alkaline CNCs suspension. The YVO_4:Eu^{3+} NPs could absorb on the surface of the chiral rods of CNCs due to the hydrogen bond and van der Waals attraction (which is confirmed by the FTIR spectra, Fig. 4). When the NPs content is low, the NPs loaded CNCs can assemble into a chiral nematic phase. However, with the increasing of NPs concentration, the NPs loaded CNCs prefers to form a disordered phase, instead. No matter how the CNCs arranges, When achiral NPs are arranged in a chiral configuration, then the CD signal should occur at the electronic excitations of the NPs, with a magnitude depending on the strength of coupling.[29]

Luminescence properties for the CY films

The excitation spectra of the CY films with different YVO_4:Eu^{3+} NPs loading exhibit broad band in the range of 230 and 360 nm (Fig. 5a), corresponding to the charge transfer transition from the VO_4^{3-} groups of the host to Eu^{3+} ions.[30] Furthermore, the charge transfer band (around 300 nm) gradually shifts to red with the increasing of YVO_4:Eu^{3+} NPs loading in cellulose matrix. This phenomenon in the CNCs based composite can be attributed to that of when the excitation energy migrates from one vanadate to the others, a part of the excitation energy will be lost due to electron-phonon coupling before it is further transferred to Eu^{3+} ion, indicating the concentration-dependence nature.[31-33] Note that in the excitation spectra the weak lines (~395, 464 nm) corresponding to the *f-f* transitions within the $4f^6$ configuration of the Eu^{3+} ions can be also observed with varying NPs content, but their intensity is relatively weak comparing with the energy transfer transitions from VO_4^{3-} to Eu^{3+}, implying the high efficiency of the energy transfer transitions.[30] Also it should be pointed out that the normalized emission spectra configuration of $^5D_0$-^7F_J transitions (J=1-4) of Eu^{3+} in the CY films remain literally the same (Fig. 5b). The quantum efficiency and photodynamic of the CY film and YVO_4:Eu^{3+} NPs are presented in Table S2 and S3 (Supporting Information), the photonic band gap dependent property occurred between these samples. The quantum efficiency obviously rises with the increase of the helical pitch, confirming that local density of the photonic structure has strong effect on it. And the photodynamic results show that the decay time of YVO_4:Eu^{3+} NPs is shorter than CY2b but longer than the CY1b and CY3b. Further

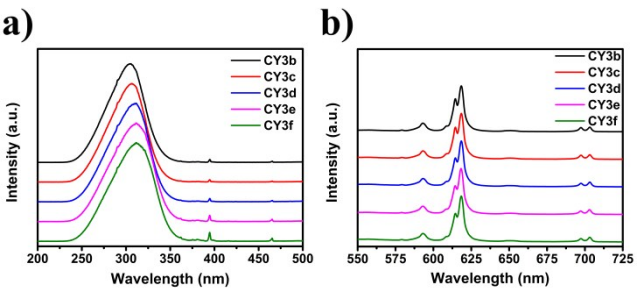

Fig. 5 (**a**) Normalized excitation spectra of the CY films monitored at 619 nm. (b) Normalized emission spectra of the CY films recorded at 303 nm.

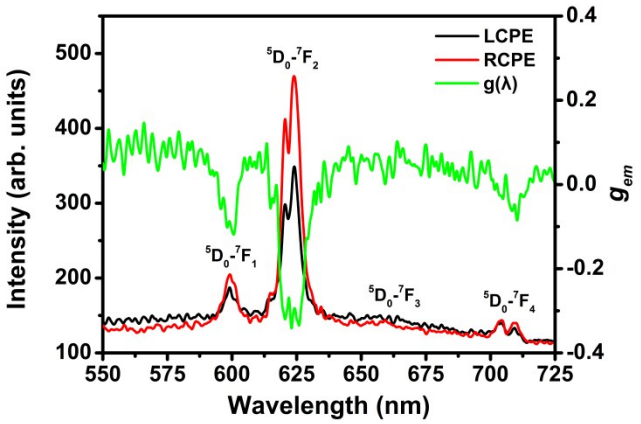

Fig. 6 The left-handed and right-handed CPE spectra of the chiral nematic CY2b, designated as LCPE and RCPE, respectively. The corresponding g_{em} calculated based on $g_{em}=2(I_L-I_R)/(I_L+I_R)$ (green line, λ_{ex}=464 nm).

investigation indicates that the photonic band gap of CY2b centered at 472 nm overlaps with the excited wavelength at 464 nm and the corresponding band gap of CY1b and CY3b centered at 342 nm and 550 nm, respectively, far away from the excited light. These results show that the corresponding photonic band gap of CY films play an important role in the luminescent dynamics.

One of the unique features of chiral nematic structure is the selective reflection of circularly polarized light that can be employed to achieve high level of CPE. The degree of circular polarization can be evaluated by luminescence polarization dissymmetry factor (g_{em}), which defined as: $g_{em}=2(I_L-I_R)/(I_L+I_R)$, where I_L and I_R are the emission intensities of the left- and right-handed polarized light, respectively. Large g_{em} values have been observed in liquid crystalline conjugated polymer and quantum dot/dye doped chiral nematic liquid crystals in solution phase,[8-11] however, as g_{em} of chiral assembled rare-earth NPs in condensed phase has never explicitly exploited, it is worth exploring the helical arrangement induced CPE properties of the CY films.

The difference in absorption for right and left circularly polarized light is obtained by measuring the difference in luminescence intensity for left and right circularly polarized exaction. As shown in Fig. 6, four *f-f* transitions of Eu^{3+} ions attribute to $^5D_0$-^7F_J (J=1-4) are observed in the right- and left-handed CPE spectra, designated as RCPE and LCPE, respectively, in the spectral range of 550-725 nm. The emission intensity of RCPE is stronger than that of LCPE because of the left-handed chiral nematic host matrix selectively reflects left-handed circularly polarized light only. The CPE of the $^5D_0$-$^7F_2$ electric-dipole transition gives the largest $|g_{em}|$ value of 0.358 and the $|g_{em}|$ value arising from the $^5D_0$-$^7F_1$ magnetic-dipole is 0.118, that is different from the chiral lanthanide complexes measured in excited electronic state, in which the g_{em} value in magnetic-dipole is bigger than that in electric-dipole.[34] The significant g_{em} value can be attributed to the integration of YVO_4:Eu^{3+} NPs into a well-defined helical chiral organization.[35]

Conclusions

In summary, we have shown the first example of a new structural design to achieve high level of CPE from an inherently achiral

YVO_4:Eu^{3+} NPs with hierarchical chiral arrangement. In this simple design only the CNCs are required as template for the host matrix. The YVO_4:Eu^{3+} NPs adhere to the surface of the CNCs nanorods through hydrogen bond and van der Waals attraction, exhibiting a helical organization as well as chiral electronic excitation. The ease and robustness of fabrication and high level of g_{em} make the current method and the composite films particularly attractive. Further experimental and computational studies are guided towards gaining insight of key governing factors of the hybrid composite films. We are convinced that this new kind of CPE material has great potential as an initial point to expend the valuable family of simple rare-earth NPs, as well as to develop smarter and better CPE-based optical device.

Acknowledgements

The authors are grateful to the funding agencies including the National Natural Science Foundation of China (21171067, 21373100), Jilin Provincial Talent Funds (802110000412) and Tang Aoqing Professor Funds of Jilin University (450091105161). Sincere gratitude goes to Prof. X.Y.Liu for POM imaging analysis.

Notes and references

[a] *State Key Laboratory of Inorganic Synthesis and Preparative Chemistry, Jilin University, 2699 Qianjin Street, Changchun 130012, China Tel: 86 431 85168607; E-mail: yanxu@jlu.edu.cn;*

[b] *State Key Laboratory of Integrated Optoelectronics, College of Electronic Science and Engineering, Jilin University, 2699 Qianjin Street, Changchun 130012, China;*

† Electronic Supplementary Information (ESI) available: [details of any supplementary information available should be included here]. See DOI: 10.1039/b000000x/

1. K. Okano, M. Taguchi, M. Fujiki and T. Yamashita, *Angew. Chem. Int. Ed.*, 2011, **123**, 12682-12685.
2. E. M. Sánchez-Carnerero, F. Moreno, B. L. Maroto, A. R. Agarrabeitia, M. J. Ortiz, B. G. Vo, G. Muller and S. d. l. Moya, *J. Am. Chem. Soc.*, 2014, **136**, 3346-3349.
3. J. Liu, H. Su, L. Meng, Y. Zhao, C. Deng, J. C. Ng, P. Lu, M. Faisal, J. W. Lam and X. Huang, *Chem. Sci.*, 2012, **3**, 2737-2747.
4. J. E. Field, G. Muller, J. P. Riehl and D. Venkataraman, *J. Am. Chem. Soc.*, 2003, **125**, 11808-11809.
5. E. Peeters, M. P. Christiaans, R. A. Janssen, H. F. Schoo, H. P. Dekkers and E. Meijer, *J. Am. Chem. Soc.*, 1997, **119**, 9909-9910.
6. J. Kumar, T. Nakashima, H. Tsumatori and T. Kawai, *J. Phys. Chem. Lett.*, 2014, **5**, 316-321.
7. G. Muller, *Dalton Trans.*, 2009, **44**, 9692-9707.
8. A. Bobrovsky, K. Mochalov, V. Oleinikov, A. Sukhanova, A. Prudnikau, M. Artemyev, V. Shibaev and I. Nabiev, *Adv. Mater.*, 2012, **24**, 6216-6222.
9. S. Chen, D. Katsis, A. Schmid, J. Mastrangelo, T. Tsutsui and T. Blanton, *Nature*, 1999, **397**, 506-508.
10. K. L. Woon, M. O'Neill, G. J. Richards, M. P. Aldred and S. M. Kelly, *Phys. Rev. E*, 2005, **71**, 041706.
11. M. Voigt, M. Chambers and M. Grell, *Chem. Phys. Lett.*, 2001, **347**, 173-177.
12. Y. Liu, D. Tu, H. Zhu and X. Chen, *Chem. Soc. Rev.*, 2013, **42**, 6924-6958.
13. S. Mukherjee and H. Woods, *Biochim. et Biophys. Acta*, 1953, **10**, 499-511.
14. Y. Habibi, L. A. Lucia and O. J. Rojas, *Chem. Rev.*, 2010, **110**, 3479-3500.
15. S. Dong and M. Roman, *J. Am. Chem. Soc.*, 2007, **129**, 13810-13811.
16. C. D. Edgar and D. G. Gray, *Cellulose*, 2001, **8**, 5-12.
17. S. Beck, J. Bouchard and R. Berry, *Biomacromolecules*, 2010, **12**, 167-172.
18. X. M. Dong, T. Kimura, J. F. Revol and D. G. Gray, *Langmuir*, 1996, **12**, 2076-2082.
19. J. Pan, W. Hamad and S. K. Straus, *Macromolecules*, 2010, **43**, 3851-3858.
20. G. Chu, J. Feng, Y. Wang, X. Zhang, Y. Xu and H. Zhang, *Dalton Trans.*, 2014, **43**, 15321-15327.
21. G. Chu, W. Xu, D. Qu, Y. Wang, H. Song and Y. Xu, *J. Mater. Chem. C*, 2014, **43**, 9189-9195
22. S. Beck-Candanedo, D. Viet and D. G. Gray, *Langmuir*, 2006, **22**, 8690-8695.
23. A. Huignard, V. Buissette, G. Laurent, T. Gacoin and J.-P. Boilot, *Chemistry of materials*, 2002, 14, 2264-2269.
24. K. E. Shopsowitz, H. Qi, W. Y. Hamad and M. J. MacLachlan, *Nature*, 2010, **468**, 422-425.
25. H. Qi, K. E. Shopsowitz, W. Y. Hamad and M. J. MacLachlan, *J. Am. Chem. Soc.*, 2011, **133**, 3728-3731.
26. A. Kuzyk, R. Schreiber, Z. Fan, G. Pardatscher, E. M. Roller, A. Högele, F. C. Simmel, A. O. Govorov and T. Liedl, *Nature*, 2012, **483**, 311-314.
27. Z. Fan and A. O. Govorov, *Nano Lett.*, 2010, **10**, 2580-2587.
28. Y. Duan and S. Che, *Chem. Eur. J.*, 2013, **19**, 10468-10472.
29. A. Ben-Moshe, B. M. Maoz, A. O. Govorov and G. Markovich, *Chem. Soc. Rev.*, 2013, **42**, 7028-7041.
30. A. Huignard, V. Buissette, A. C. Franville, T. Gacoin and J. P. Boilot, *J. Phys. Chem. B*, 2003, **107**, 6754-6759.
31. L. Xie, H. Song, Y. Wang, W. Xu, X. Bai and B. Dong, *J. Phys. Chem. C*, 2010, **114**, 9975-9980.
32. H. Althues, P. Simon and S. Kaskel, *J. Mater. Chem.*, 2007, **17**, 758-765.
33. D. Hreniak, J. Doskocz, P. GŁuchowski, R. Lisiecki, W. Stręk, N. Vu, D. Loc, T. Anh, M. Bettinelli and A. Speghini, *J. Lumin.*, 2011, **131**, 473-476.
34. M. Iwamura, Y. Kimura, R. Miyamoto and K. Nozaki, *Inorg. Chem.*, 2012, **51**, 4094-4098.
35. F. Song, G. Wei, X. Jiang, F. Li, C. Zhu and Y. Cheng, *Chem. Commun.*, 2013, **49**, 5772-5774.